P2.12 VARIATION OF OCEANIC RAIN RATE PARAMETERS FROM SSM/I: MODE OF BRIGHTNESS TEMPERATURE HISTOGRAM

Roongroj Chokngamwong and Long Chiu*
Center for Earth Observing and Space Research, George Mason University,
Fairfax, VA 22030-4444 USA

1. INTRODUCTION

Oceanic precipitation is a major component in the global hydrologic cycle and plays an important role in climate processes. The oceans cover about 70 percent of the earth's surface, absorbing the sun's energy and releasing it in the form of longwave flux, sensible heat flux and latent heat flux (evaporation). Most of the oceanic evaporation returns to the oceans as oceanic precipitation. The atmosphere transports the residue water vapor to continental areas over which most are deposited as continental precipitation. Excess continental precipitation over evapotranspiration results in runoffs. The cycle is completed by the return of the excess water to the oceans through surface and ground water runoffs.

Climate changes associated with global warming have been investigated. Analyses of observation and model simulations show a general increase of surface temperature. Consensus show that the earth's surface temperature has risen by about 0.5°C (or 1°F) in the past century. This change is consistent with model simulations of an enhanced hydrological cycle associated with a warmer climate (Wetherald and Manabe, 2002). Kumar et al. (2004) examined data and model simulations and showed that while tropical oceanic precipitation increases in phase with sea surface temperature changes, land precipitation actually decreases.

To better understand the response of the earth's climate to the hydrological cycle, analyses of a long-term hydrologic variables data are needed. Due to the scarcity of gauge networks, remote sensing data are the only means available for monitoring precipitation over the global oceans.

Wilheit et al. (1991) developed a technique for estimating monthly oceanic rain rates based on Special Sensor Microwave Imager (SSM/I) measurements taken on board the Defense Meteorological Satellite Program (DMSP) satellites. In the algorithm, the observed microwave brightness temperature (T_b) histogram is fitted to a mixed lognormal rain rate distribution. The non-raining part of the T_b distribution is described by T_0 and σ_0, which are the mean and standard deviation of the T_b for the non-raining portion of the T_b histogram. The raining part of the distribution is described by the rain fraction (p), and the mean and standard deviation of the conditional rain rate distribution. This data set is an input to the global rainfall maps developed by the Global Precipitation Climatology Project (Huffman et al. 1997), hence its variability must be quantified for an accurate assessment of climate variabilities. This data set is fairly homogeneous-all estimates are based on measurements from identical sensors, although the orbital parameters are slightly different.

In this paper, we document the seasonal, interannual and long term trends of T_0 based on Empirical Orthogonal Function (EOF), trend analyses of the non-seasonal T_0 and Empirical Mode Decomposition (EMD) analyses of the zonal averages.

2. DATA SETS

The data set used in this study is the oceanic monthly rain rates produced at the Global Precipitation Climatology Project (GPCP) - Polar Satellite Precipitation Data Center (PSPDC) using the technique developed by Wilheit et al. (1991). The 17-year (1988-2004) data are derived from the SSM/I on board the DMSP satellites. The DMSP satellites are in sun synchronous orbits at an altitude of about 800 km. The orbital characteristics of DMSP satellites are described in the table 1. Two monthly data sets are available: a 5° x 5° monthly data set for the ascending and descending DMSP satellite passes, respectively, covering the area from 50°N to 50°S and a 2.5° x 2.5° monthly data set covering 65°N to 65°S. The data can be obtained from the GPCP-PSPDC website [URL: http://gpcp-pspdc. gmu.edu].

* *Corresponding author address*: NASA/Goddard Space Flight Center, GES Data and Information and Services Center, Greenbelt, MD 20771; e-mail: lchiu@gmu.edu.

Satellite	Ascending Time (At Launch)	Altitude (km)	Eccentricity	Orbital Period (mins)	Temporal Coverage
F08	06:15	851-832	0.00132	101.8	Jul 1987 – Dec 1991
F11	18:11	878-841	0.00129	101.9	Jan1992 – Apr 1995
F13	17:42	856-844	0.00083	102.0	May 1995 – Present

Table 1. The orbital characteristics of DMSP Satellites and the temporal coverage of the data sets (DMSP platform description URL: http://nsidc.org/data/docs/daac/f13_platform.gd.html). Orbit inclination is 98.8º for all three satellites.

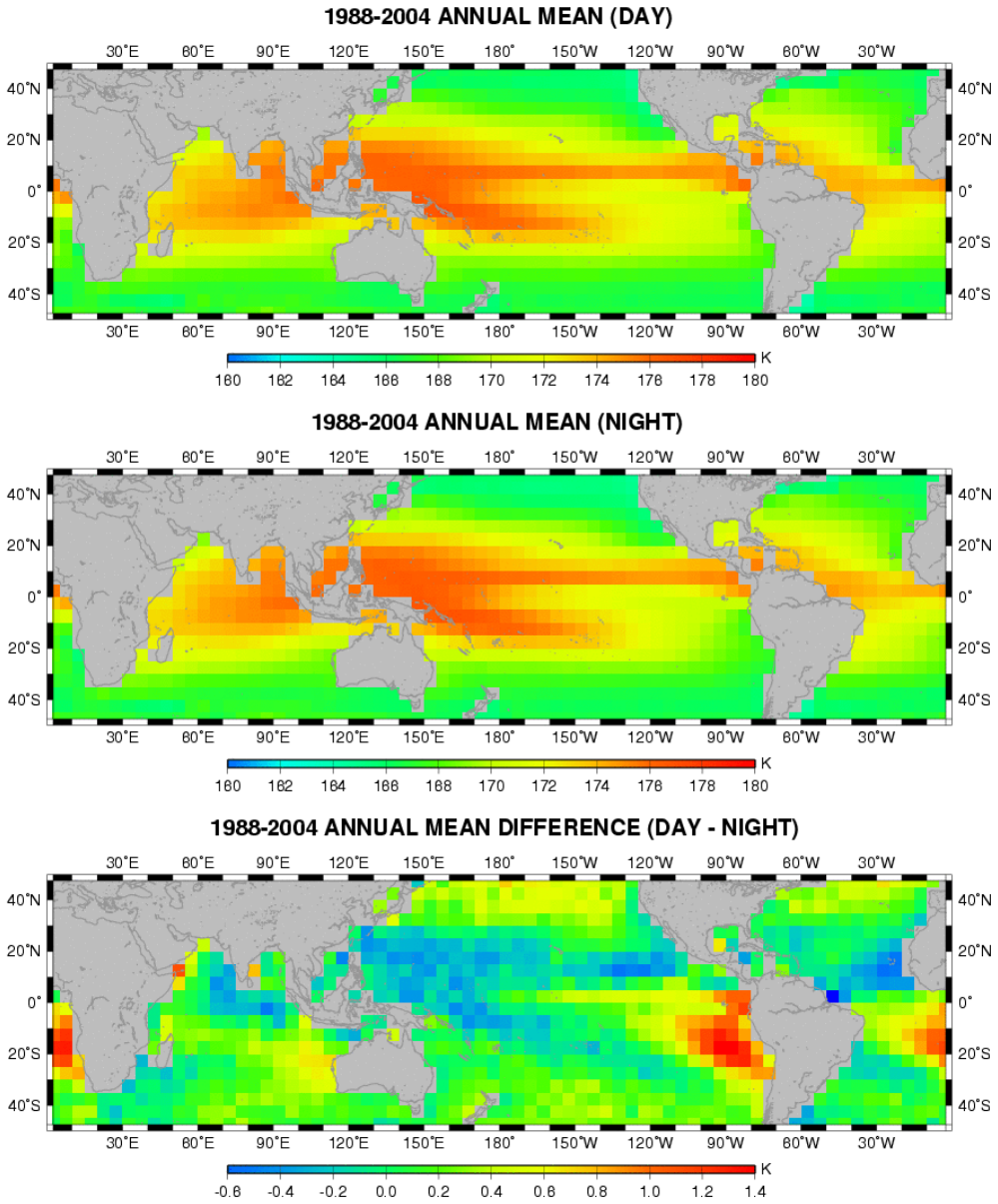

Figure 1. The distribution of T_0 for daytime and nighttime and the diurnal difference over the global ocean

Wilheit et al.'s (1991) technique fits the histograms of SSM/I T_b to a mixed rain rate distribution via a rain rate - T_b relation derived from radiative transfer calculations based on an atmospheric model. In the atmospheric model, a constant lapse rate of 6.5°C/km and a linear increase of the relative humidity from 80% at the ocean surface to 100% at the freezing level are assumed. The variations of sea surface temperature and emissivity due to surface wind are neglected. The rain rate distribution consists of a raining part with probability of p and a nonraining part with probability of (1-p). A lognormal distribution is assumed for the raining part. The fitting of the T_b histogram is based on three moments of the distributions (mean, variance and skewness). Kedem et al. (1990) reported that the rain rate above 1 mm/hr observed from the Global Atmospheric Research Program (GARP) Atlantic Tropical Experiment (GATE) could be fitted to a lognormal distribution quite well. The SSM/I has seven channels at four frequencies (19.35, 22.235, 37 and 85.5 GHz). A linear combination channel ($2T_{19v} - T_{22v}$) is used in this algorithm to reduce the impact of variability of water vapor. A Gaussian distribution of T_b is assumed for the nonraining part of the histogram with a mean T_0 and a standard deviation σ_0. At each iteration, all parameters, T_0, σ_0, p and the mean and standard variation of the conditional rain rates, are modified to minimize the errors between the moments. T_0 is also used to adjust the difference between the observed and computed T_b histograms.

The rain rate, r (in mm/hr) can be empirically related to T_b via the following relationship:

$$T_b(r) = T_0 + (285 - T_0)(1 - e^{r/r_c}) - 3.5r^{1/2}$$

where r_c is $25/FL^{1.2}$ and FL is the freezing height (in kilometers) of the rain layer (Wilheit et al., 1991). T_b increases with rain rates in the lower rain rates (the emission regime), but decreases for higher rain rates due to scattering of the hydrometeors. Sensor biases between satellites can contribute to biases in rainfall estimates. Since T_b increases with rain rate for the frequently observed rain rate range, a low bias in T_b would result in a lower rain rate, and vice versa.

3. RESULTS

3.1 *Climatology of T_0*

Figure 1 shows the distribution of annual mean of the daytime and nighttime T_0 of the SSM/I and the difference between them. High T_0 regions coincide with high rain areas such as the Intertropical Convergence Zone (ITCZ) and the South Pacific Convergence Zone (SPCZ). The spatial patterns of the daytime and nighttime T_0 are very similar. The maximum (day-night) difference of 1.47K occurs over the oceanic dry regions, where the rain probability is less than 1%. Over the ITCZ and the SPCZ, daytime T_0 tends to be lower with a maximum difference of -0.6K.

Figure 2 shows the zonal average T_0. The zonal maximum of about 175K is found in the latitude belt between 5°N-10°N for both daytime and nighttime T_0. This latitude coincides with the maximum zonal oceanic precipitation (Chiu and Chang, 1994). In the southern hemisphere, zonal average daytime T_0 is higher than the nighttime T_0.

Figure 3 shows the seasonal climatology of zonal average T_0. Both daytime and nighttime T_0 show a maximum of about 176K in June at 5°N-10°N and decrease to higher latitudes to about less than 164K. This pattern is similar to earlier results based on 1987-1993 data (Chiu and Chang, 1994). The zonal average T_0 shows a distinct seasonal cycle with minima in the summer.

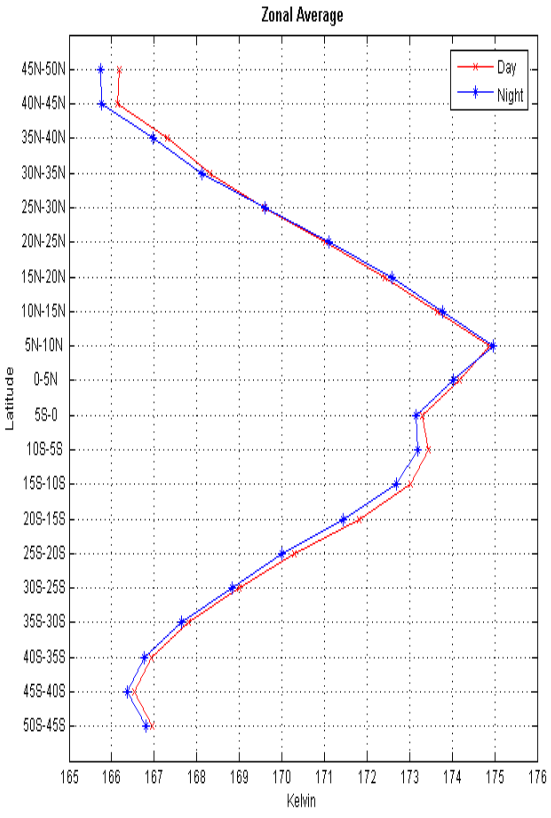

Figure 2. Zonal annual average of T_0

3.2 *Empirical Orthogonal Function (EOF) Analyses*

An Empirical Orthogonal Function (EOF) analysis was performed on the non-seasonal T_0 to extract the dominant modes of variations. The first two EOF patterns are presented in Figure 4. These patterns are significant by the test proposed by North et al. (1982). The patterns are similar between the daytime and nighttime data. The first EOF patterns have the same (negative) sign everywhere, characterized by large variability at the equator. The nighttime EOF1 shows a stronger latitudinal contrast than the daytime EOF1. The time series associated with the EOF1 pattern noticeably show distinct jumps that are characterized by the satellite changes. The second EOF patterns are characterized by strong variations at the equatorial central pacific. This pattern is similar to the ENSO pattern of oceanic precipitation found earlier (Chang et al., 1993). The time series associated with the EOF patterns are shown in figure 5. The associated time series of the EOF2 pattern are correlated to a Southern Oscillation Index (SOI) at -0.67 and -0.68 for daytime and nighttime data, respectively.

3.3 *Trend Analysis*

Figure 6 shows the time series of global average daytime and nighttime T_0. Linear regression analyses show that both time series show slight linear decreasing trend of about 0.8K over 17 years.

We applied Empirical Mode Decomposition (EMD) to examine "trends" in the zonal average time series. EMD is an adaptive technique that decomposes a time series into intrinsic mode functions (IMFs). The decomposition is based on the extraction of variance associated with various intrinsic time scales selected from the time series. The EMD can deal with both non-linear and non-stationary data. Each IMF will present different oscillations in the data and the last mode or the residual will show the "trend" of the data. By the "trend" we mean monotonic variation of the time series that shows the longest time scale. In the present work, the EMD is used to extract the components of T_0 to study its interannual variation. The EMD analyses of the zonal averages show no "trends" in most of the latitudes, except decreasing trends of about 2K and 1K between 40°N-50°N and between 30°S-40°S for the daytime and 1K between 40°N-50°N for the nighttime.

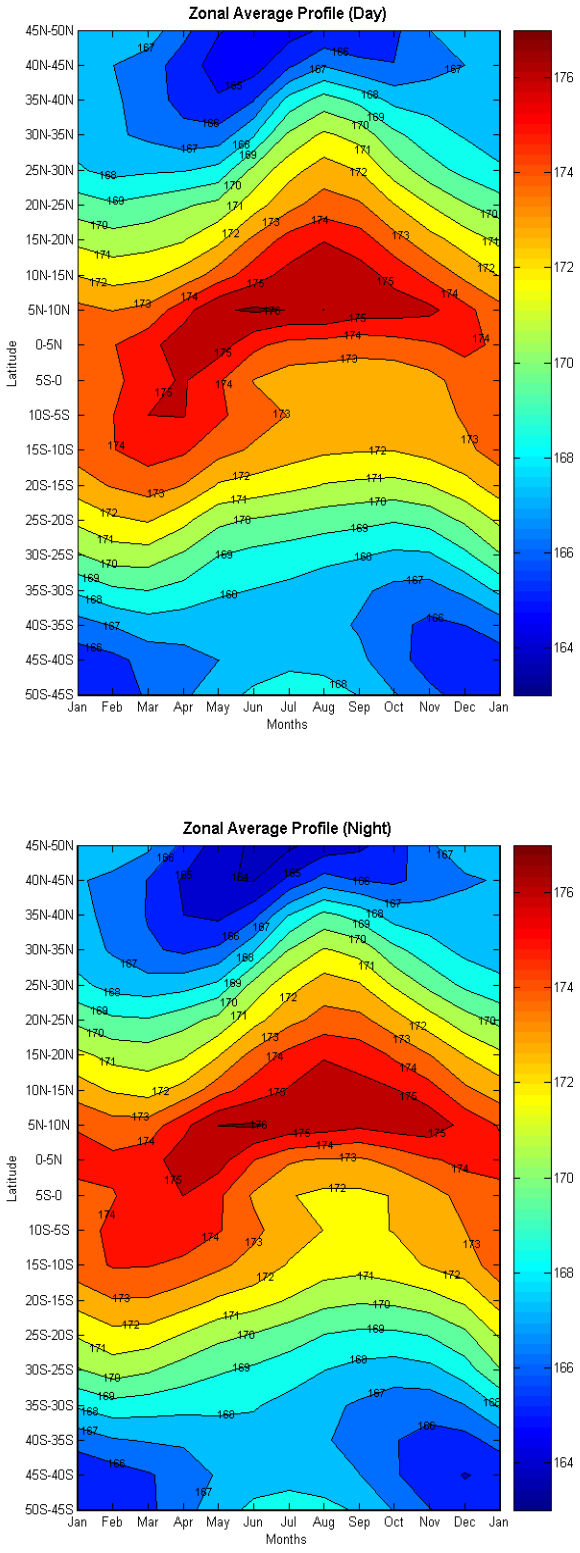

Figure 3. Zonal climatology of T_0 (day and night)

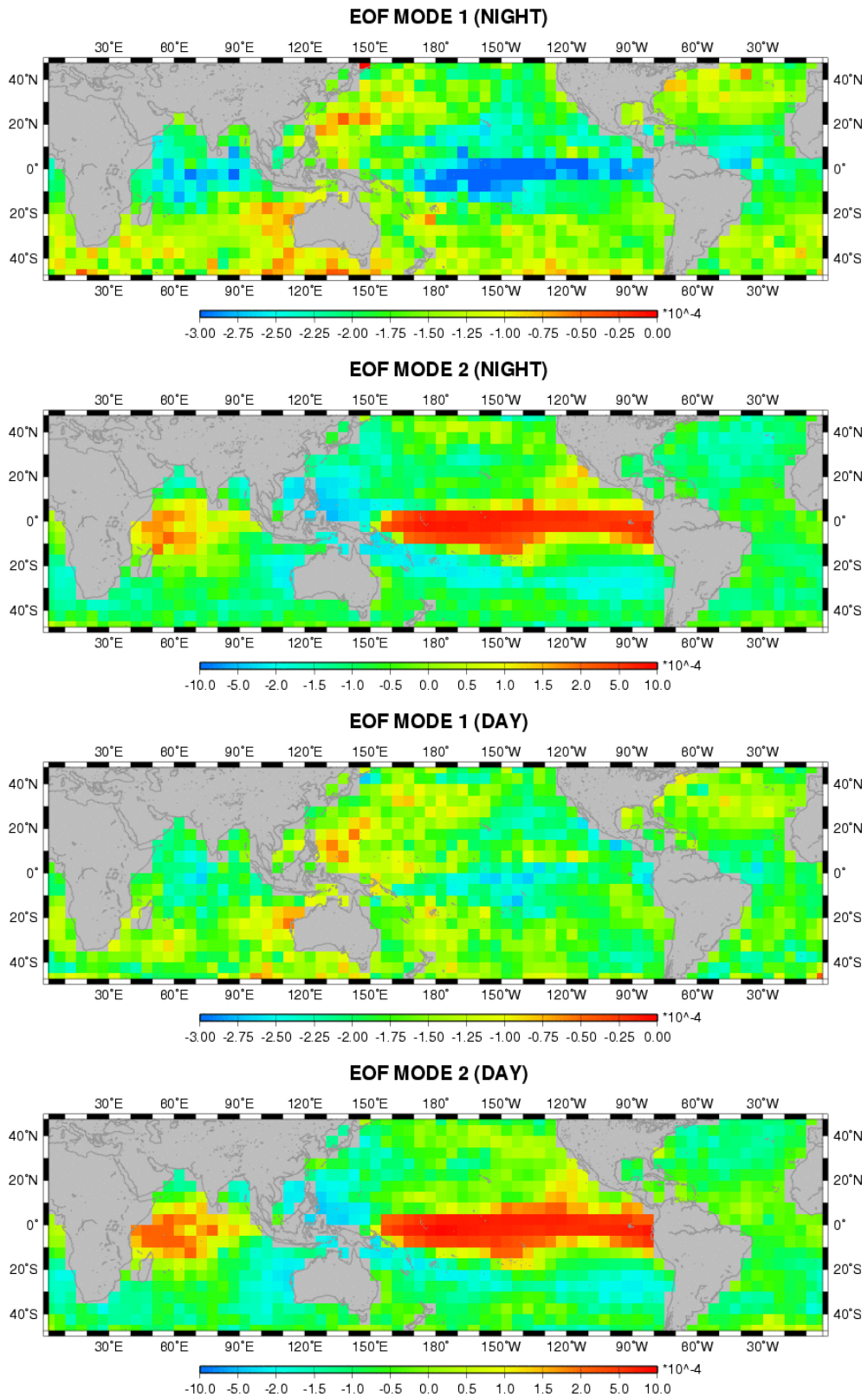

Figure 4. EOF patterns of nonseasonal T_0 for daytime and nighttime

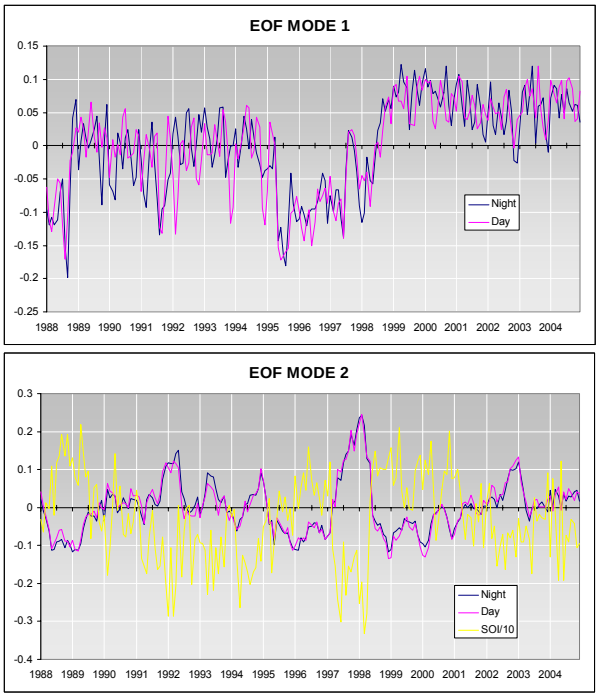

Figure 5. Time series associated with EOF patterns

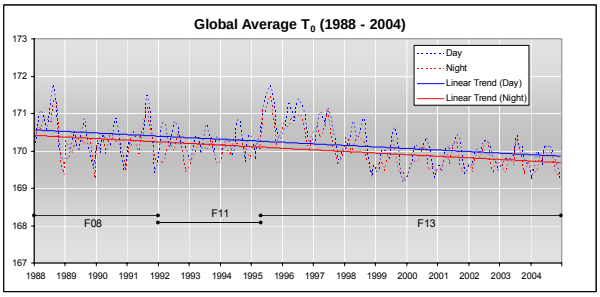

Figure 6. Time series of global average T_0 and linear trend analysis.

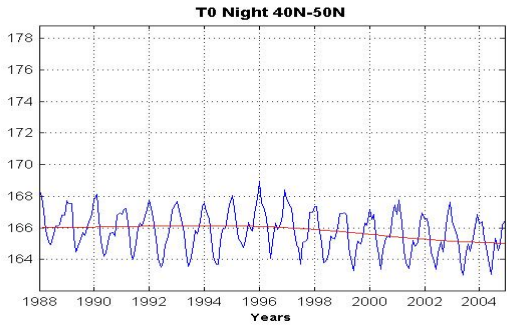

Figure 7. Highest Intrinsic Mode Function of EMD analysis of nighttime zonal average T_0 at 40°N-50°N

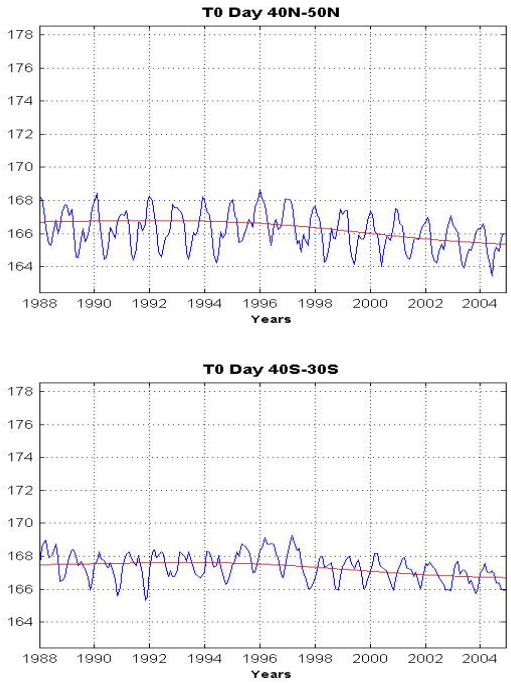

Figure 8. Same as Figure 7, except for daytime zonal average T_0 at 40°N-50°N and 30°S-40°S

4. SUMMARY AND DISCUSSIONS

T_0 is the average T_b of the combination channel for non-raining observations. Wilheit et al. (1990) found that T_0 is very stable globally for the first 15 months of operation. Regional and interannual variability is attributed to variations in surface wind, sea surface temperature, columnar water vapor and cloud liquid water. T_0 is also the T_b of zero rain rate in the T_b-rain rate relation. A low bias in the calibrated T_b will result in lower T_0 and therefore lower rain rates.

The daytime and nighttime climatology of T_0 are similar. The equator to pole difference is about 10K and the maximum seasonal amplitude is ~8-10K at mid-latitudes. The maximum (day-night) difference of 1.47K occurs in the oceanic dry regions. Spatial pattern of T_0 is similar to the oceanic precipitation pattern- high T_0 areas are found in the heavy rain areas such as the ITCZ and the SPCZ. In these regions, nighttime T_0 is higher than daytime T_0, consistent with the observations of a nocturnal or early morning maximum in diurnal rainfall (Chang et al., 1995). The maximum zonal average T_0 is found in the latitude 5°N-10°N. There is an asymmetry of zonal average T_0 in the tropics, with maximum T_0 occurring in August in the northern hemisphere and in April-May in the southern hemisphere.

EOF analyses of the non-seasonal daytime and nighttime T_0 show that the EOF1 is a spatially coherent pattern (same sign everywhere). The associated time series show a distinct jump (of ~1K), coinciding with the changes of the F11 to F13 satellite. The impact of this jump on precipitation rates needs to be quantified.

An ENSO signal is found in the second EOF patterns, similar to the pattern observed in non-seasonal precipitation variations (Chang et al., 1993). Their associated time series show high correlations with an ENSO index.

New et al. (2001) found that between 1950 and 2000, oceanic precipitation between 30°S-30°N decreases at a rate of -6.42 mm/decade, according to limited gauge observations. Kumar et al. (2004) show an increase in oceanic precipitation associated with an increase in sea surface temperature. We have performed EMD and trend analysis of the zonal mean precipitation processed by the GPCP-PSPDC. Our results (not shown here) show that there is no significant "trends" in the zonal mean rain rate except for a significant (10%) increasing "trend" between 0-10°N, in the deep tropics. Since T_0 shows decreasing "trends" in the extra-tropics, they cannot be contributing to the "trends" in tropical precipitation. In order to quantify the "trends" in oceanic precipitation, we are examining other rain rate parameters, such as fractional and conditional rain rate, and height of the rain column.

The time series of global average T_0 show a decreasing trend of 0.8K. The trend may be attributed to changes in the satellites. EMD analyses show no "trends" in the zonal average T_0 except for decreasing trends at the high latitudes, between 40°N-50°N for both daytime and nighttime and between 30°S-40°S for nighttime T_0. These decreasing "trends" in the extra-tropics suggest rainfall decrease in the subtropics. If we consider these decreases in conjunction with increasing "trends" in precipitation in the deep tropics, this pattern is consistent with the decadal enhancement of the Hadley circulation, as argued by other investigators (Wielicki et al., 2002; Cess and Udelhofen, 2003; Chiu and Xing, 2004).

ACKNOWLEDGMENTS

The processing of SSM/I oceanic rain rate is supported by NASA as part of its contribution to the WCRP GPCP program. LSC is supported by NASA TRMM program and RC is supported by a GRA from the Center for Earth Observing and Space Research at George Mason University.

REFERENCES

Cess, R.D. and P.M. Udelhofen, 2003: Climate change during 1985-1999: Cloud interactions determined from satellite measurements. *Geophysical Research Letter*, 30, 1019-1022

Chang, A.T.C., L.S. Chiu and T. Wilheit, 1993: Oceanic monthly rainfall derived from SSM/I. *Eos, Trans. Amer. Geophys. Union*., 74, 505-513

Chang, A.T.C., L.S. Chiu and G. Yang, 1995: Diurnal cycle of oceanic precipitation from SSM/I data. *Mon. Wea. Rev.*, 123, 3371-3380

Chiu, L.S. and Y. Xing, 2004: Modes of Interannual Variability of Oceanic Evaporation Observed From GSSTF2. *Int. J. Biodiversity, Oceanology and Conservation*, Vol. 68, No. 2, 115-120

Chiu, L.S. and T.C. Chang, 1994: Oceanic Rain Rates Parameters Derived From SSM/I. *Climatic Parameters In Radiowave Propagation and Prediction (CLIPARA94),* Moscow

Huffman, G., R. Adler, P. Arkin, A. Chang, R. Ferraro, A. Gruber, J. Janowiak, A. McNab, B. Rudolph and U. Schneider, 1997: The Global Precipitation Climatology Project (GPCP) Combined Precipitation Dataset, *Bul. Amer. Meteor. Soc.*, 78, 5-20.

Kedem, B., L. Chiu and G. North, 1990: Estimation of mean rain rates: Applications to satellite observations. *J. Geophys. Res.*, 95, 1965-1972

Kumar, A., Y. Fanglin, G. Lisa and S. Siegfried, 2004: Differing Trends in the Tropical Surface Temperatures and Precipitation over Land and Oceans. *J. Climate,* 17, 653-664

New, M., M. Todd, M. Hulme and P. Jones, 2001: Precipitation Measurements and Trends in The Twentieth Century. *Int. J. Climatol.*, 21, 1899-1922

North, G.R., T.L. Bell, R.F Cahalan and F.J. Meong, 1982: Sampling Errors in the Estimation of Empirical Orthogonal Functions. *Mon. Wea. Rev*., 110, 699-706

Wetherald, R., and S. Manabe, 2002: Simulaiton of hydrologic changes associated with global warming, *J. Geophys. Res*., 107 (D19), 4379

Wielicki, B., T. Wong, R.P. Allen, A. Slingo, J.T. Kiehl, R.J. Soden, C.T. Gordon, A.J. Miller, S-K Yang, D.A. Randall, F. Robsertson, J.Susskind and H. Jacobowitz, 2002: Evidence for large decadal variability in the tropical mean radiative energy budget. Science, 295 (5556), 841-844

Wilheit, T.T., A.T.C. Chang and L.S. Chiu, 1991: Retrieval of Monthly Rainfall Indices from Microwave Radiometric Measurements Using Probability Distribution Functions. *J. Atmos. Oceanic Technol.*, 8, 118-136